
Cooperative diagnostics for combinations of large volume metrology systems

Domenico Augusto Maisano* and
Luca Mastrogiacommo

Politecnico di Torino,
Department of Management and Production Engineering (DIGEP),
Corso Duca degli Abruzzi 24, 10129, Torino, Italy
Email: domenico.maisano@polito.it
*Corresponding author

Abstract: Recent studies show that the combined use of large-volume metrology (LVM) systems (e.g., laser trackers, rotary-laser automatic theodolites, photogrammetric systems, etc.) can lead to a systematic reduction in measurement uncertainty and a better exploitation of the available equipment. The objective of this paper is to present some diagnostic tests for combinations of LVM systems that are equipped with distance and/or angular sensors. Two are the tests presented: a *global* test to detect the presence of potential anomalies during measurement and a *local* test to isolate any faulty sensor(s). This diagnostics is based on the *cooperation* of sensors of different nature, which merge their local measurement data, and it can be implemented in real-time, without interrupting or slowing down the measurement process. The description of the tests is supported by several experimental examples.

[Submitted 28 March 2017; Accepted 27 December 2017]

Keywords: large-volume metrology; LVM; distributed sensors; multi-system combination; cooperative diagnostics; statistical test; measurement consistency.

Reference to this paper should be made as follows: Maisano, D.A. and Mastrogiacommo, L. (2019) 'Cooperative diagnostics for combinations of large volume metrology systems', *Int. J. Manufacturing Research*, Vol. 14, No. 1, pp.15–42.

Biographical notes: Domenico Augusto Maisano is an Associate Professor of Quality Engineering at the Politecnico di Torino. His research interests are quality engineering/management, large-volume metrology, indicators and scientometrics. He is a member of the editorial board of the *Quality Engineering Journal* and has co-authored four monographs and more than 100 publications in international journals/proceedings.

Luca Mastrogiacommo is an Associate Professor of Production Systems at the Politecnico di Torino. His research interests are in the field of industrial metrology, quality management and statistical process control. He has co-authored two books and more than 70 published papers in international journals and conference proceedings.

1 Introduction

The field of *large-volume metrology* (LVM) deals with objects with linear dimensions ranging from several metres to tens of metres (Estler et al., 2002; Peggs et al., 2009; Franceschini et al., 2011; Schmitt et al., 2016). Typical industrial applications concern dimensional verification and assembly of large-sized mechanical components, in which levels of uncertainty of several tenths of millimetre are generally tolerated (Maropoulos et al., 2014; Chen et al., 2015). These applications are typically performed using technologically advanced LVM systems, which are very expensive and may require time consuming set-up and measurement operations (Franceschini and Maisano, 2014).

LVM systems are usually equipped with *sensors* able to perform local measurements of distances and/or angles. Depending on the sensor layout, LVM systems can be classified into:

- 1 *centralised*, if sensors are grouped into a unique stand-alone unit (e.g., a laser tracker)
- 2 *distributed*, if sensors are spread around the measurement volume [e.g., a set of rotary-laser automatic theodolites (Maisano et al., 2008)].

Even though the existing measuring systems may differ in technology and metrological characteristics, two common features are:

- 1 the use of some *targets* to be localised, which are generally mounted on a hand-held probe for localising the points of interest or in direct contact with the measured object's surface
- 2 the fact that target localisation is performed using local measurements by sensors.

For distributed LVM systems, sensors are arranged around the measured object and there are three possible approaches for target localisation (Franceschini et al., 2011):

- *multilateration*, using the *distances* between targets and sensors
- *multiangulation*, using the *angles* subtended by targets with respect to sensors
- *hybrid techniques*, which are based on the combined use of angles and distances between targets and sensors.

Although several types of LVM systems are (not rarely) available in the same industrial workshop or metrology laboratory, they are often used independently of each other (e.g., a laser tracker is used for certain tasks, a photogrammetric system for others, and so on). This is a rather myopic view because it ignores the benefits that may result from the combination of multiple systems, including but not limited to:

- overcoming the limitations of the individual systems
- improving measurement accuracy and coverage
- reducing the risk of measurement errors, due to measurement redundancy.

Franceschini et al. (2016) recently proposed a novel approach, in which a combination of LVM systems that are equipped with sensors of different nature – i.e., sensors with different metrological characteristics and able to measure distances and/or angles – share

their measurement data and cooperate for determining a unique localisation of the target. In other words, data provided by a number of sensors from different LVM systems are fused together in order to localise the target (Galletto et al., 2015; Franceschini et al., 2016; Maisano and Mastrogiacomo, 2016). According to this philosophy, the set of (centralised and/or distributed) LVM systems that are used in conjunction can be seen as a single distributed LVM ‘macro-system’, consisting of sensors of different nature.

The purpose of this article is to present some statistical tests, which provide a practical online diagnostics functionality. These tests allow to detect possible measurement anomalies and, subsequently, isolate any potentially faulty sensor(s). This diagnostics can be classified as *cooperative*, since it is based on the cooperation of sensors of different nature.

In detail, two statistical tests will be discussed:

- a *global* test, aimed at evaluating the consistency of the target localisation, based on the variability of the local measurements by sensors
- a *local* test that – when a target localisation is not considered consistent by the global test – identifies the potentially faulty sensor(s) and (temporarily) excludes them from the target-localisation process, without interrupting it.

These tests can be interpreted as a generalisation of similar tests that have been previously developed: i.e.,

- 1 some tests for distributed LVM systems with distance sensors only
- 2 other tests for distributed LVM systems with angular sensors only; in this sense, this research represents an important update of (Franceschini et al., 2009, 2014).

The remainder of this paper is structured into four sections. Section 2 provides some background information, which is helpful to grasp the subsequent description of statistical tests, precisely:

- 1 basic concepts concerning diagnostics
- 2 a synthetic description of the target-localisation mathematical model in use.

Section 3 provides a detailed description of the statistical tests, with several experimental examples. Section 4 summarises the original contributions of this research, focusing on its implications, limitations and possible future developments. Details on the mathematical model for target localisation are contained in the Appendix.

2 Background information

2.1 Basic concepts concerning diagnostics

In general, the concept of *consistency of a measurement* is defined as follows. For each measurable quantity x , we can define a confidence interval $[LL, UL]$ (where LL stands for lower limit and UL for upper limit). The measure (\hat{x}) of the quantity x is considered consistent if $\hat{x} \in [LL, UL]$ (Gertler, 1998; Franceschini et al., 2011).

The type-I and type-II probability errors (misclassification rates) respectively correspond to:

$$\begin{aligned}\alpha &= \Pr\{\hat{x} \notin [LL, UL] \mid \text{absence of systematic error sources}\} \\ \beta &= \Pr\{\hat{x} \in [LL, UL] \mid \text{presence of systematic error sources}\}\end{aligned}\tag{1}$$

Usually, LL and UL reflect the natural variability of the measurement system (which is related to the metrological characteristics of *accuracy*, *reproducibility*, *repeatability*, etc.), in the absence of systematic error sources¹ (JCGM 200:2008, 2008).

For distributed systems, local anomalies in one or more sensors can distort or even compromise the target localisation. On the other hand, when these anomalies are recognised, the target-localisation results can be corrected by (temporarily) excluding malfunctioning sensor(s). This is the reason why distributed systems are – to some extent – rather ‘vulnerable’ but can be successfully protected by appropriate diagnostic tools.

The diagnostics presented in this paper can be classified as *cooperative*, since the sensor local measurements are used in conjunction: not only for localising the target but also for detecting possible measurement anomalies/accidents in this process. As mentioned in Section 1, this diagnostics includes two tests (global and local), aimed respectively at

- 1 identifying inconsistent localisations
- 2 identifying and (temporarily) excluding purportedly faulty sensors.

2.2 Mathematical model for target localisation

This section briefly recalls a recent mathematical model for target localisation, when using combinations of LVM systems equipped with sensors of different nature. In general, each i^{th} LVM system (S_i) includes a number of sensors; we conventionally indicate the generic j^{th} sensor of S_i as s_{ij} (e.g., s_{i1} , s_{i2} , ..., s_{ij} , ...). Sensors can be classified in two typologies:

- *distance* sensors, able to measure their distance (d_{ij}) from the target (see Figure A2, in the Appendix)
- *angular* sensors, able to measure the azimuth (θ_{ij}) and elevation (ϕ_{ij}) angle subtended by the target (see Figure A2, in the Appendix).

Assuming that P is the point to be localised in the 3D space (e.g., the centre of a spherical target), the localisation problem may be formulated through the following linear (or linearised) model (Galletto et al., 2015; Franceschini et al., 2016):

$$A \cdot X - B \equiv \begin{bmatrix} A^{dist} \\ A^{ang} \end{bmatrix} \cdot X - \begin{bmatrix} B^{dist} \\ B^{ang} \end{bmatrix} = 0\tag{2}$$

where $X = [X, Y, Z]^T$ is the position vector of P in a global Cartesian coordinate system $OXYZ$; A^{dist} , A^{ang} and B^{dist} , B^{ang} are respectively the so-called *design* and *reduced measured* observation matrices, both referred to $OXYZ$ (Wolberg, 2005). The matrices related to distance sensors are labelled with superscript ‘dist’, while those related to

angular sensors with superscript ‘ang’. \mathbf{A} and \mathbf{B} contain several parameters related to each generic $(ij)^{\text{th}}$ sensor: the position/orientation parameters (X_{0ij} , Y_{0ij} , Z_{0ij} and ω_{ij} , ϕ_{ij} , κ_{ij}) and the distance (d_{ij}) and/or angles (θ_{ij} , φ_{ij}) subtended by the target, with respect to a local Cartesian coordinate system $o_{ij}x_{ij}y_{ij}z_{ij}$. Since the ‘true’ values of the above parameters are never known exactly, they can be replaced with appropriate estimates: \hat{X}_{0ij} , \hat{Y}_{0ij} , \hat{Z}_{0ij} , $\hat{\omega}_{ij}$, $\hat{\phi}_{ij}$ and $\hat{\kappa}_{ij}$ resulting from initial calibration process(es), \hat{d}_{ij} resulting from distance measurements, $\hat{\theta}_{ij}$ and $\hat{\varphi}_{ij}$ and resulting from angular measurements. For details on the construction of \mathbf{A} and \mathbf{B} , see Section A1 (in the Appendix).

The unknown coordinates of P are determined solving the system in equation (2), which is generally *overdefined*, i.e., there are more equations than unknown parameters: one for each distance sensor and two for each angular sensor.

The equations of the system may differently contribute to the uncertainty in the localisation of P . Three important factors affecting this uncertainty are:

- 1 *Uncertainty in the local measurements* (\hat{d}_{ij} , $\hat{\theta}_{ij}$ and $\hat{\varphi}_{ij}$) by sensors, which generally depends on their metrological characteristics.
- 2 *Relative position* between P and each sensor; e.g., for angular sensors, the uncertainty in the localisation of P increases proportionally to the distance between P and the sensors (Maisano and Mastrogiacono, 2016).
- 3 *Uncertainty in the position/orientation of sensors*, resulting from initial calibration process(es).

For simplicity, the proposed mathematical model considers only the first two factors, neglecting the third one (Maisano and Mastrogiacono, 2016).

Having said that, it would be appropriate to solve the system in equation (2) giving greater weight to the contributions from the sensors producing less uncertainty and *vice versa*. To this purpose, a practical method is that of *generalised least squares* (GLS) (Franceschini et al., 2011; Kariya and Kurata, 2004), in which a weight matrix (\mathbf{W}), which takes into account the uncertainty produced by the equations, is defined as:

$$\mathbf{W} = [\mathbf{J} \cdot (\mathbf{cov}(\boldsymbol{\xi})) \cdot \mathbf{J}^T]^{-1} \quad (3)$$

where \mathbf{J} is the Jacobian matrix containing the partial derivatives of the elements in the first member of equation (2) (i.e., $\mathbf{A} \cdot \mathbf{X} - \mathbf{B}$) with respect to the sensors’ local measurements (contained in the vector $\boldsymbol{\xi}$), and $\mathbf{cov}(\boldsymbol{\xi})$ is the relevant covariance matrix. For details, see Section A1 in the Appendix.

Assuming that sensors work independently from each other and there is no correlation between the local measurements related to different sensors, $\mathbf{cov}(\boldsymbol{\xi})$ is a diagonal matrix containing the variances related to these measurements. Variances can be determined in several ways:

- 1 from manuals or technical documents relating to the sensors in use
- 2 estimated through *ad hoc* experimental tests
- 3 estimated using data from previous calibration processes.

We remark that these values should reflect the sensors' uncertainty in realistic working conditions, e.g., in the presence of vibrations, light/temperature variations and other typical disturbance factors.

By applying the GLS method to the system in equation (3), we obtain the final estimate of \mathbf{X} as:

$$\hat{\mathbf{X}} = (\mathbf{A}^T \cdot \mathbf{W} \cdot \mathbf{A})^{-1} \cdot \mathbf{A}^T \cdot \mathbf{W} \cdot \mathbf{B} \quad (4)$$

For further details on the GLS method, see Kariya and Kurata (2004).

3 Online diagnostic tests

This section is organised into two subsections: Section 3.1 describes a *global* test to evaluate the consistency of a target localisation, while Section 3.2 describes a *local* test that – when a target localisation is not considered consistent by the global test – identifies the potentially faulty sensor(s) and (temporarily) excludes them from the localisation process, without interrupting it.

Before going into the discussion of the tests, we define the *residuals* of the sensor local measurements as the difference between the measured quantities (labelled with the symbol ‘^’) and those calculated using the coordinates of P , resulting from the localisation process [see equations (A3) and (A7), in the Appendix]:

$$\left. \begin{aligned} \varepsilon_{d_{ij}} &= \hat{d}_{ij} - d_{ij} \\ \varepsilon_{\theta_{ij}} &= \hat{\theta}_{ij} - \theta_{ij} \\ \varepsilon_{\varphi_{ij}} &= \hat{\varphi}_{ij} - \varphi_{ij} \end{aligned} \right\} \begin{array}{l} \text{for distance sensors} \\ \text{for angular sensors} \end{array} \quad (5)$$

In the absence of systematic error causes, it is reasonable to hypothesise that these residuals follow zero-mean normal distributions: $\varepsilon_{d_{ij}} \sim N(\mu_{d_{ij}} \approx 0, \sigma_{d_{ij}}^2)$, $\varepsilon_{\theta_{ij}} \sim N(\mu_{\theta_{ij}} \approx 0, \sigma_{\theta_{ij}}^2)$ and $\varepsilon_{\varphi_{ij}} \sim N(\mu_{\varphi_{ij}} \approx 0, \sigma_{\varphi_{ij}}^2)$; these hypotheses will be tested experimentally. The dispersion of residuals (depicted by the relevant variances $\sigma_{d_{ij}}^2$, $\sigma_{\theta_{ij}}^2$ and $\sigma_{\varphi_{ij}}^2$) depends on the technical/metrological characteristics of sensors; e.g., measurements performed using technologically advanced sensors, such as the interferometer or absolute distance metre (ADM) of a laser tracker, are likely to be less dispersed than those performed using relatively coarse sensors, such as ultrasonic distance sensors or low-end photogrammetric cameras.

Assuming that $\sigma_{d_{ij}}^2$, $\sigma_{\theta_{ij}}^2$ and $\sigma_{\varphi_{ij}}^2$ are known, residuals can be standardised as follows:

$$\left. \begin{aligned} z_{d_{ij}} &= \frac{\varepsilon_{d_{ij}} - \mu_{d_{ij}}}{\sigma_{d_{ij}}} \approx \frac{\varepsilon_{d_{ij}}}{\sigma_{d_{ij}}} \\ z_{\theta_{ij}} &= \frac{\varepsilon_{\theta_{ij}} - \mu_{\theta_{ij}}}{\sigma_{\theta_{ij}}} \approx \frac{\varepsilon_{\theta_{ij}}}{\sigma_{\theta_{ij}}} \\ z_{\varphi_{ij}} &= \frac{\varepsilon_{\varphi_{ij}} - \mu_{\varphi_{ij}}}{\sigma_{\varphi_{ij}}} \approx \frac{\varepsilon_{\varphi_{ij}}}{\sigma_{\varphi_{ij}}} \end{aligned} \right\} \begin{array}{l} \text{for distance sensors} \\ \text{for angular sensors} \end{array} \quad (6)$$

The resulting standardised residuals are, by definition, normally distributed random variables with zero mean and unit variance: $z_{d_{ij}}, z_{\theta_{ij}}, z_{\phi_{ij}} \sim N(0, 1)$.

3.1 Global test

The first diagnostic criterion is aimed at identifying the non-plausible localisations of P. The standardised residuals related to the sensors involved in the target localisation [see equation (6)] are aggregated into the *standardised residual sum of squares* (SRSS) indicator:

$$SRSS(P) = \sum_{ij \in I^{dist}} z_{d_{ij}}^2 + \sum_{ij \in I^{ang}} (z_{\theta_{ij}}^2 + z_{\phi_{ij}}^2) = \sum_{ij \in I^{dist}} z_{d_{ij}}^2 + \sum_{ij \in I^{ang}} z_{\theta_{ij}}^2 + \sum_{ij \in I^{ang}} z_{\phi_{ij}}^2 \quad (7)$$

where I^{dist} and I^{ang} are the sets of index-pair values (ij), relating to the sensors able to perform distance and angular measurements respectively. In general, these types of local measurements are mutually exclusive, since sensors able to measure distances are not able to measure angles and *vice versa*.

By definition, $SRSS(P) \geq 0$ for all the points (P) in the measurement volume. Since the localisation problem is overdetermined and sensor measurements are naturally dispersed, a solution that exactly satisfies all distance and angular constraints (i.e., $SRSS(P) = 0$) is not realistically possible.

In a broader perspective, $SRSS(P)$ is the sum of $|I^{dist}|$, $|I^{ang}|$ and $|I^{ang}|$ squared realisations (the symbol ' $| \cdot |$ ' denotes the cardinality of a set) of the zero-mean and unit-variance normally distributed random variables $z_{d_{ij}}, z_{\theta_{ij}}$ and $z_{\phi_{ij}}$. $SRSS(P)$ can therefore assume the following form:

$$SRSS(P) = \chi_{d_{ij}}^2 + \chi_{\theta_{ij}}^2 + \chi_{\phi_{ij}}^2 \quad (8)$$

where $\chi_{d_{ij}}^2, \chi_{\theta_{ij}}^2$ and $\chi_{\phi_{ij}}^2$ are three chi-square distributed random variables, with respectively $|I^{dist}|$, $|I^{ang}|$ and $|I^{ang}|$ degrees of freedom (DoF), since they are obtained by summing independent terms.

$SRSS(P)$ is a new chi-square distributed random variable with $|I^{dist}| + |I^{ang}| + |I^{ang}| = |I^{dist}| + 2 \cdot |I^{ang}|$ DoF, since it is obtained by adding the three above chi-square distributed variables (Ross, 2009).

Every time the localisation of a target is performed, diagnostics calculates the quantity $SRSS(P)$. Assuming a risk α as a type-I error, a one-sided confidence interval for $SRSS(P)$ can be calculated in order to test the consistency of the localisation; $\chi_{v, 1-\alpha}^2$ is the upper limit of this interval, considering a chi-square distribution with $v = |I^{dist}| + 2 \cdot |I^{ang}|$ DoF and a $(1 - \alpha)$ confidence level.

The test drives to the following two alternative conclusions:

$$SRSS(P) \leq \chi_{v, 1-\alpha}^2 \rightarrow \text{localisation is considered consistent}$$

$$SRSS(P) > \chi_{v, 1-\alpha}^2 \rightarrow \text{localisation is considered inconsistent, hence it is rejected.}$$

3.1.1 Set up of test parameters

The risk level α is established by the user. A high α prevents from dubious localisations, although it might drive to reject good ones. On the other hand, a low α speeds up the localisation process, although it might drive to collect wrong data due to the consequent increase of the type-II error (β).

The variances of residuals – which are essential for calculating the standardised residuals – can be determined empirically, localising a sample of M points randomly distributed in the measurement volume, in the absence of systematic error sources. For each k -th point, the three types of residuals defined in equation (5) can be calculated: $\varepsilon_{d_{ij}}$, $\varepsilon_{\theta_{ij}}$ and $\varepsilon_{\varphi_{ij}}$. The number of residuals of each type may change depending on the number of sensors involved in each k^{th} localisation, which is in turn influenced by their communication range and relative position with respect to P (Maisano and Mastrogiacomo, 2016).

In the absence of systematic error causes and time or spatial/directional effects, it is reasonable to assume that homologous residuals – i.e., residuals concerning the same type of measured quantity (\hat{d}_{ij} , $\hat{\theta}_{ij}$ and $\hat{\varphi}_{ij}$), from sensors of the same (i^{th}) LVM system – are zero-mean normally distributed random variables with the same dispersion. This is justified by the fact that the local-measurement dispersion of sensors is closely related to their technical and metrological characteristics.

Therefore, the mean values and variances of the residuals of the problem are reduced to:

$$\begin{aligned} \mu_{d_{i\bullet}}, \sigma_{d_{i\bullet}}^2 & \text{ for the } \varepsilon_{d_{ij}} \text{ residuals} \\ \mu_{\theta_{i\bullet}}, \sigma_{\theta_{i\bullet}}^2 & \text{ for the } \varepsilon_{\theta_{ij}} \text{ residuals} \\ \mu_{\varphi_{i\bullet}}, \sigma_{\varphi_{i\bullet}}^2 & \text{ for the } \varepsilon_{\varphi_{ij}} \text{ residuals} \end{aligned} \tag{9}$$

where the subscript ' $i\bullet$ ' indicates that these parameters are calculated aggregating the residuals related to sensors from the i^{th} LVM system (S_i), considering the totality of the localisations of the M points available. The resulting mean values can be used to test the hypothesis of zero-mean distributions, while the variances can be used to determine the standardised residuals for the test [see equation (6)].

3.1.2 First experimental example

In a first example, let us consider a specific combination of two LVM prototype systems:

- (S_1) MScMS-I, i.e., a system consisting of multiple ultrasonic sensors – denominated Crickets (Franceschini et al., 2010) – which are able to measure their distance from the target.
- (S_2) MScMS-II, i.e., a system consisting of different toy cameras – PixArt/WiiMote infrared cameras, with 126·96 pixels resolution and 100 fps – which are able to measure the angles subtended by the target (Franceschini et al., 2011).

Both systems have been designed and developed at Politecnico di Torino – DIGEP and include inexpensive but not very accurate sensors, e.g., the typical distance-measurement uncertainty of Crickets is of the order of a few millimetres (Franceschini et al., 2010),

while the angular-measurement uncertainty of the toy cameras is of the order of some tenths of a degree (Maisano and Mastrogiacomo, 2016).

We set up a distributed LVM ‘macro-system’ consisting of five Crickets (i.e., s_{11} , s_{12} , s_{13} , s_{14} and s_{15}) and three toy cameras (i.e., s_{21} , s_{22} and s_{23}) with known positions and orientations, which are distributed around the measurement volume, as schematised in Figure 1.

The variances of the residuals were estimated empirically, considering a sample of about $M = 50$ points, which are randomly distributed in the measurement volume. The localisation of these points was performed in a controlled environment (e.g., temperature, light and vibrations were kept under control) and the distributions of residuals were thoroughly analysed, in order to exclude measurement accidents, e.g., time or spatial/directional effects, or non-random causes of variation in general.

Since all the MScMS-I distance sensors as well as the MScMS-II angular sensors are nominally identical, residuals can be grouped into three sets: one (including the $\varepsilon_{d_{1j}}$ residuals) for the distance sensors from S_1 , and two (including the $\varepsilon_{\theta_{2j}}$ and $\varepsilon_{\varphi_{2j}}$ residuals) for the angular sensors from S_2 . The zero-mean normal distribution of these sets of residuals was verified by the Anderson-Darling normality test at $p < 0.05$ (Ross, 2009).

Table 1 reports the mean and standard-deviation values estimated for these sets of residuals.

Table 1 Estimated mean value and variance related to the local-measurement residuals, in the first experimental example

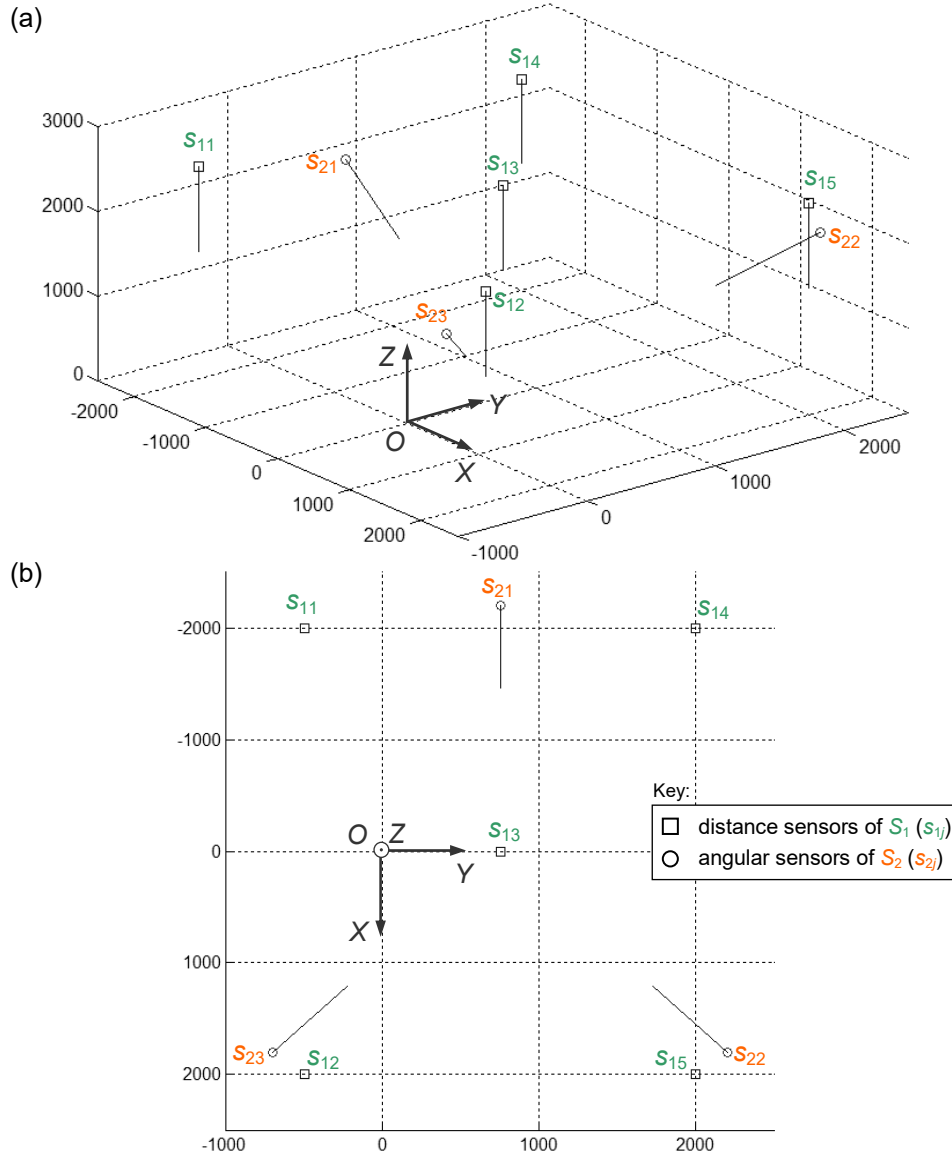
<i>Residuals</i>	<i>Sensors</i>	<i>Number</i>	<i>Mean value</i>	<i>Variance</i>
$\varepsilon_{d_{1j}}$	$s_{11}, s_{12}, s_{13}, s_{14}$ and s_{15}	$5 \cdot 50 = 250$	$\hat{\mu}_{d_{1\cdot}} = -0.05 \text{ mm}$	$\hat{\sigma}_{d_{1\cdot}}^2 = 3.38 \text{ mm}^2$
$\varepsilon_{\theta_{2j}}$	s_{21}, s_{22} and s_{23}	$3 \cdot 50 = 150$	$\hat{\mu}_{\theta_{2\cdot}} = 0.02 \text{ deg}$	$\hat{\sigma}_{\theta_{2\cdot}}^2 = 0.083 \text{ deg}^2$
$\varepsilon_{\varphi_{2j}}$	Idem	Idem	$\hat{\mu}_{\varphi_{2\cdot}} = -0.038 \text{ deg}$	$\hat{\sigma}_{\varphi_{2\cdot}}^2 = 0.090 \text{ deg}^2$

In conditions of maximum visibility – i.e., all the five distance sensors and three angular sensors are able to see the target P – the confidence-interval limit for SRSS, assuming a type-I risk level $\alpha = 0.05$ and $\nu = |I^{dist}| + 2 \cdot |I^{ang}| = 5 + 2 \cdot 3 = 11$ DoF, becomes:

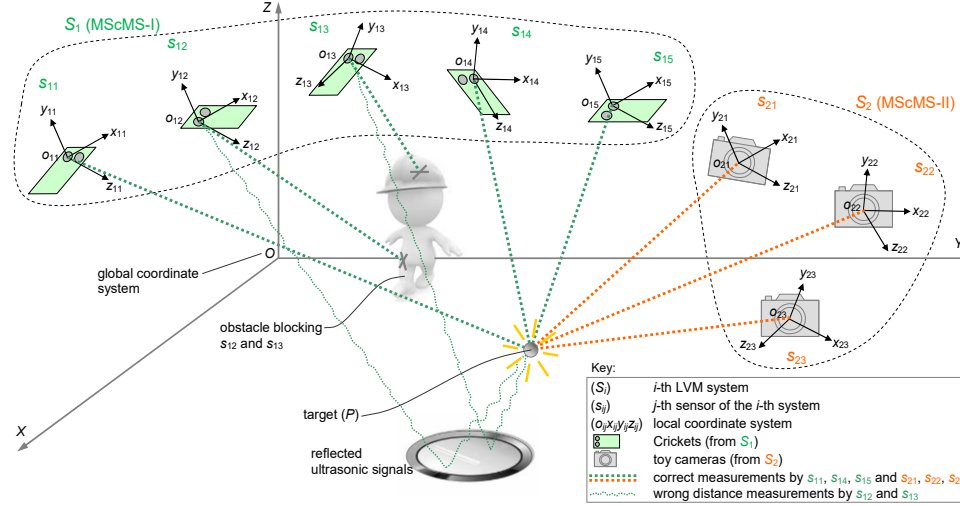
$$SRSS(P) \leq \chi_{\nu=11, 1-\alpha=0.95}^2 \Rightarrow SRSS(P) \leq 19.7 \quad (10)$$

Let us now consider a possible accident that can occurs using ultrasonic sensors. Referring to the representation in Figure 2, suppose that an obstacle, for example an operator who performs the measurement, is interposed between P and two of the distance sensors (i.e., s_{12} and s_{13}), blocking them. At the same time, the ultrasonic signal reflection on the floor/ceiling of the workshop produces two wrong measurements. Consequently, the distance measurements by s_{12} and s_{13} are significantly overestimated. Also, it is assumed that the remaining sensors are able to perform their local measurements correctly; see the example in Table 2(a).

Figure 1 Representation of the position and orientation of the distance (s_{1j}) and angular (s_{2j}) sensors in use in the first experimental example, (a) 3D view (b) XY plane view (see online version for colours)



Notes: $OXYZ$ is the global coordinate system (coordinates in millimetres).
The outgoing vectors (in blue) represent the sensor orientations.

Figure 2 Scheme of the set-up in the first experimental example (see online version for colours)

Note: A measurement accident in two (ultrasonic) sensors (i.e., s_{12} and s_{13}) of S_1 causes wrong distance measurements (d_{12} and d_{13}).

In this case, the mathematical model will produce the following (distorted) localisation solution: $P \equiv (-99.9, 1449.7, 21.2)$ [mm], which is characterised by a high error: $SRSS(P) \approx 1.2 \cdot 10^5 > 19.7$. Owing to this result, the global test suggests that this localisation is inconsistent.

Table 2 Example of local measurements by the sensors of a combination of two LVM systems (S_1 and S_2) in the first experimental example, (a) in the presence of an accident causing wrong distance measurements by s_{12} and s_{13} (b) after removing the cause of the accident

Sensor	(a) Accident present			(b) Accident removed		
	d_{ij} [mm]	θ_{ij} [deg]	φ_{ij} [deg]	d_{ij} [mm]	θ_{ij} [deg]	φ_{ij} [deg]
s_{11}	3,272.6	N/A	N/A	3,274.6	N/A	N/A
s_{12}	(Wrong) 4,236.5	N/A	N/A	(Correct) 2,814.9	N/A	N/A
s_{13}	(Wrong) 3,196.3	N/A	N/A	(Correct) 1,970.4	N/A	N/A
s_{14}	3,314.0	N/A	N/A	3,318.1	N/A	N/A
s_{15}	2,857.1	N/A	N/A	2,856.8	N/A	N/A
s_{21}	N/A	13.37	-29.36	N/A	13.42	-29.36
s_{22}	N/A	-10.33	-34.35	N/A	-10.23	-34.46
s_{23}	N/A	122.80	-35.86	N/A	122.91	-35.83

After removing the obstacle, the new distances related to s_{12} and s_{13} are respectively $d_{12} = 4236.5$ mm and $d_{13} = 3196.3$ mm, while the local measurements relating to the remaining sensors are almost identical to the previous ones [see Table 2(b)]. The new localisation is: $P \equiv (352.7, 698.6, 560.6)$ [mm]. The corresponding SRSS value is $SRSS(P) \approx 4.44 \leq 19.7$. Hence, the new localisation can be considered consistent.

3.1.3 Second experimental example

Let us consider a second example in which two LVM systems include sensors with relatively high metrological characteristics. Precisely, these two systems are:

- (S_1) A distributed photogrammetric system consisting of three Hitachi Gigabit Ethernet photogrammetric infrared cameras (s_{11} , s_{12} and s_{13}) – pixel resolution: $1,360 \times 1,024$, frame rate: 30 fps (Hitachi Kokusai Electric Inc., 2016) – using a 38.1 mm reflective spherical target. Each camera is able to provide the azimuth (θ_{11} , θ_{12} , and θ_{13}) and elevation (φ_{11} , φ_{12} , and φ_{13}) angular measurements with respect to the target P .
- (S_2) A laser tracker API RadianTM (API, 2016) with a spherically mounted retroreflector (SMR) of the same diameter of the target of S_1 . S_2 is equipped with an ADM (s_{21}), providing distance measurements (d_{21}) and an angular sensor (s_{22}), providing two angular measurements – i.e., azimuth (θ_{22}) and elevation (φ_{22}) – of P . The local Cartesian coordinate systems of the two sensors are coincident.

We set up a distributed LVM ‘macro-system’ consisting of total five sensors (i.e., s_{11} , s_{12} , s_{13} , s_{21} and s_{22}) with known positions and orientations, which are distributed around the measurement volume, as schematised in Figure 3.

The proposed localisation model is able to estimate the 3D position of each measured point, based on the nine local measurements available (i.e., two angular measurements for each of the three photogrammetric cameras; two angular measurements and one distance measurement for the laser tracker).

The mean values and variances related to the local-measurement residuals were estimated on the basis of the localisation of $M = 50$ points, which are randomly distributed in the measurement volume. The resulting values are reported in Table 3.

Table 3 Estimated mean value and variance related to the local-measurement residuals, in the second experimental example

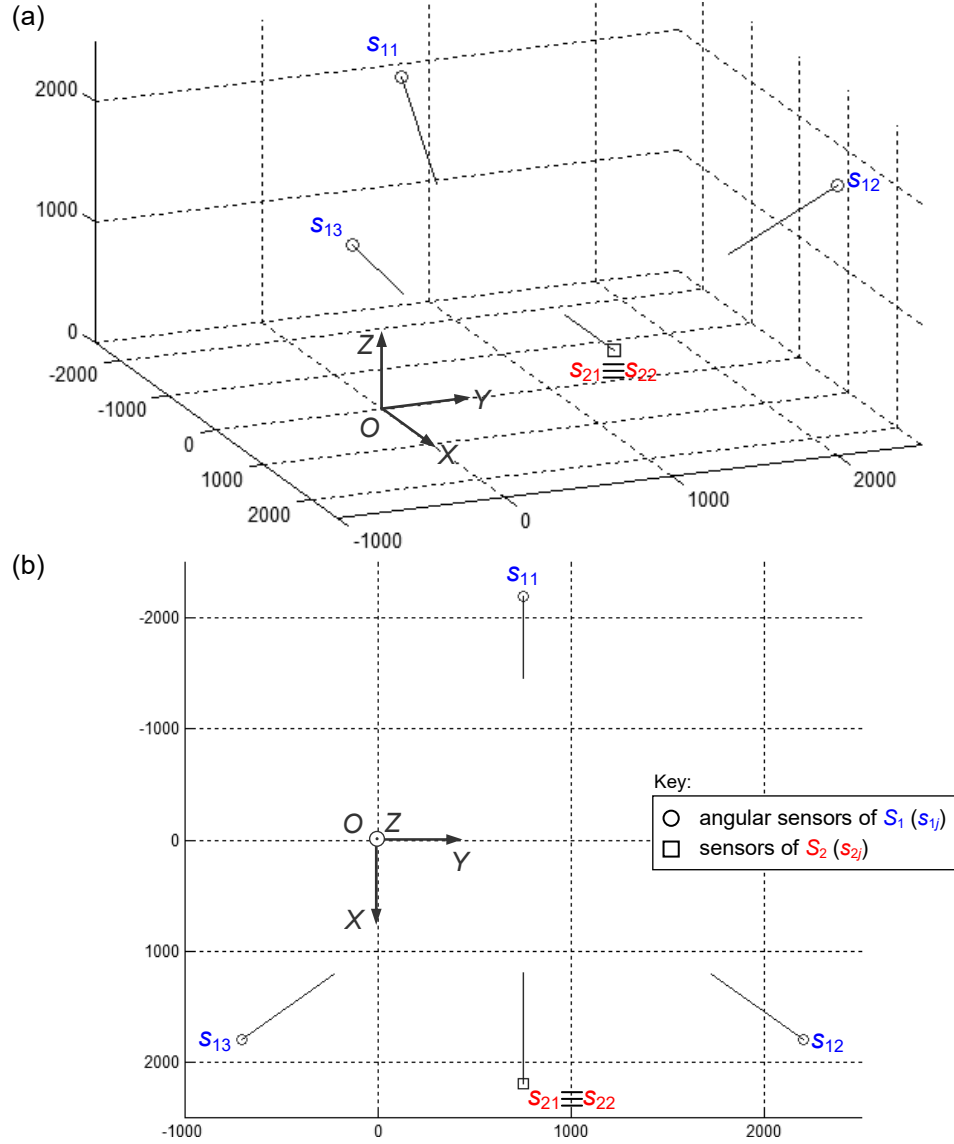
<i>Residuals</i>	<i>Sensors</i>	<i>Number</i>	<i>Mean value</i>	<i>Variance</i>
$\varepsilon_{\theta_{1j}}$	s_{11}, s_{12} and s_{13}	$3 \cdot 50 = 150$	$\hat{\mu}_{\theta_{1j}} = 1.9 \cdot 10^{-4} \text{ deg}$	$\hat{\sigma}_{\theta_{1j}}^2 = 2.5 \cdot 10^{-4} \text{ deg}^2$
$\varepsilon_{\varphi_{1j}}$	Idem	$3 \cdot 50 = 150$	$\hat{\mu}_{\varphi_{1j}} = 2.0 \cdot 10^{-4} \text{ deg}$	$\hat{\sigma}_{\varphi_{1j}}^2 = 2.6 \cdot 10^{-4} \text{ deg}^2$
$\varepsilon_{d_{2j}}$	s_{21}	50	$\hat{\mu}_{d_{2j}} = -4.5 \cdot 10^{-7} \text{ mm}$	$\hat{\sigma}_{d_{2j}}^2 = 9.1 \cdot 10^{-11} \text{ mm}^2$
$\varepsilon_{\theta_{2j}}$	s_{22}	50	$\hat{\mu}_{\theta_{2j}} = 1.1 \cdot 10^{-3} \text{ deg}$	$\hat{\sigma}_{\theta_{2j}}^2 = 3.7 \cdot 10^{-3} \text{ deg}^2$
$\varepsilon_{\varphi_{2j}}$	Idem	50	$\hat{\mu}_{\varphi_{2j}} = 8.7 \cdot 10^{-3} \text{ deg}$	$\hat{\sigma}_{\varphi_{2j}}^2 = 1.7 \cdot 10^{-3} \text{ deg}^2$

In conditions of maximum visibility (i.e., when the totality of the sensors can see the target) and assuming a type-I risk level $\alpha = 0.05$ and $\nu = 2 \cdot 3 + 1 + 1 \cdot 2 = 9$ DoF, the confidence-interval limit for SRSS becomes:

$$SRSS(P) \leq \chi_{\nu=9, 1-\alpha=0.95}^2 \Rightarrow SRSS(P) \leq 16.9 \quad (11)$$

Suppose that a possible accident produces a distortion in the angles measured by the angular encoder of the laser tracker (s_{22}), while the distance sensor (s_{21}) performs the measurement correctly (see the representation in Figure 4). Moreover, suppose that the three photogrammetric cameras (s_{11} , s_{12} and s_{13}) are able to measure the angles subtended by P correctly (see Table 4).

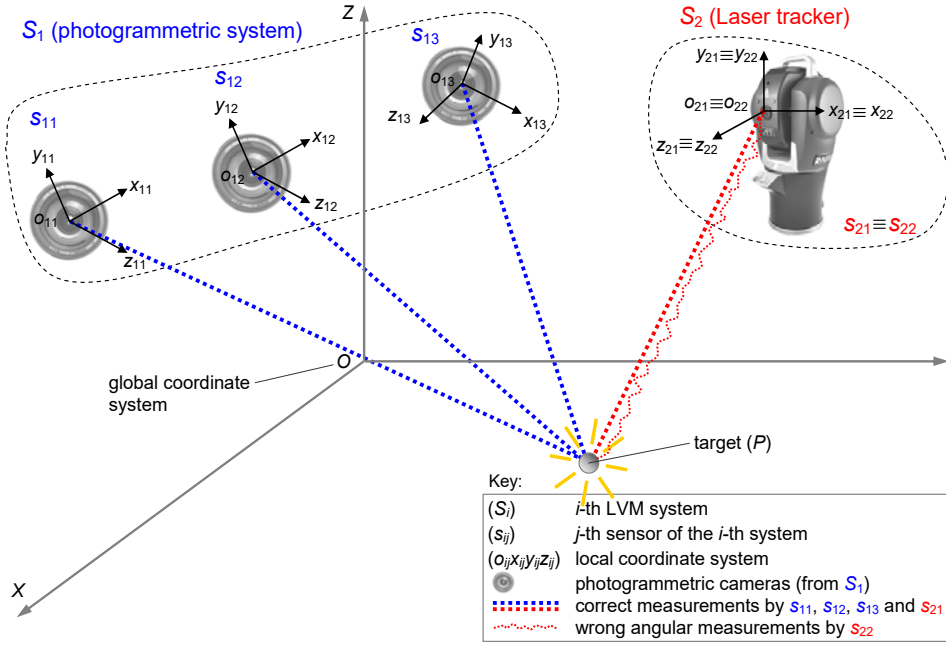
Figure 3 Representation of the position and orientation of the photogrammetric cameras (s_{1j}) and the laser-tracker distance (s_{21}) and angular (s_{22}) sensors in use in the second experimental example, (a) 3D view (b) XY plane view (see online version for colours)



Notes: $OXYZ$ is the global coordinate system (coordinates in millimetres).

The outgoing vectors (in blue) represent the sensor orientations.

In this case, the localisation algorithm will produce the following (distorted) localisation solution: $P \equiv (1964.9, 1254.5, 946.5)$ [mm], characterised by a high error, i.e., $SRSS(P) \approx 3.6 \cdot 10^3 > 16.9$. This diagnostic test therefore suggests to reject the localisation result.

Figure 4 Scheme of the set-up in the second experimental example (see online version for colours)

Note: A measurement accident in the laser-tracker angular sensor (s_{22}) causes the wrong measurement of the azimuth (θ_{22}) and elevation (φ_{23}) angles.

Table 4 Example of local measurements by the sensors of a combination of two LVM systems (S_1 and S_2) in the second experimental example, (a) before (b) after removing the cause of the measurement accident

Sensor	(a) Accident present			(b) No accident		
	d_{ij} [mm]	θ_{ij} [deg]	φ_{ij} [deg]	d_{ij} [mm]	θ_{ij} [deg]	φ_{ij} [deg]
s_{11}	N/A	62.16	-13.91	N/A	62.17	-13.79
s_{12}	N/A	96.95	-47.04	N/A	96.91	-47.07
s_{13}	N/A	-14.82	-27.82	N/A	-14.79	-27.80
s_{21}	559.2	N/A	N/A	559.2	N/A	N/A
s_{22}	N/A	(Wrong) 25.96	(Wrong) -7.39	N/A	(Correct) 30.96	(Correct) -3.39

Repeating the measurement after having eliminated the anomaly in s_{22} , the new angles measured by s_{22} are $\theta_{22} = 30.96$ degrees and $\varphi_{22} = -3.39$ degrees respectively, while those relating to the remaining sensors are almost identical to the previous ones [see Table 2(b)]. The new localisation is: (1952.3, 1250.3, 966.9) [mm]. The corresponding $SRSS$ value is $SRSS(P) \approx 5.23 \leq 16.9$. Hence, the new localisation can be considered consistent.

3.2 Local test

If the global test fails, a local test can be performed for failure isolation. The philosophy of this other test is to correct the results of a dubious localisation, by excluding the purportedly faulty sensor(s), without losing the observations from the remaining sensors. In this way, the target localisation process is not interrupted, even in the presence of local anomalies.

Referring to the local measurements by each $(ij)^{\text{th}}$ sensor, we now consider the three types of standardised residuals, which are defined in equation (6) (z_{dij} , $z_{\theta ij}$, and $z_{\varphi ij}$). These residuals can be used for outlier detection with uncorrelated and normally distributed observations: if the local measurement is not an outlier, then the corresponding standardised residual will be normally distributed $\sim N(0, 1)$. Each standardised residual is compared to a $\alpha/2$ -quantile and a $(1 - \alpha/2)$ -quantile of the standard normal distribution (i.e., $z_{\alpha/2}$ and $z_{1-\alpha/2}$), with the significance level α . The null-hypothesis, which denotes that the $(ij)^{\text{th}}$ local measurement is not an outlier, is rejected if the standardised residual is not included in the $[z_{\alpha/2}, z_{1-\alpha/2}]$ symmetrical confidence interval. An outlier in one standardised residual generally causes ones other residuals to be increased in absolute values.

Local testing is easy under the assumption that there is only one purportedly faulty sensor (or outlier) in the current localisation: the local measurement with the largest (absolute value of the) standardised residual, provided that it is beyond the confidence interval, is regarded as an outlier and the corresponding sensor (s_{ij}) is excluded from the localisation problem.

The assumption that there is only one outlier is a severe restriction in the case measurements from more than one sensor are degraded. However, the procedure can be extended to multiple outliers iteratively: after the exclusion of a potentially faulty sensor, the statistical test and the rejection of one other sensor can be repeated until no more outliers are identified (Wieser et al., 2004).

3.2.1 Set up of test parameters

The standardised residuals that are used in this test are the same that are used in the global test; therefore they can be calculated according to the procedure described in Section 3.

3.2.2 First application example

Returning to the example presented in Section 3.1.2 – in which two distance sensors (s_{12} and s_{13}) perform distorted measurements – the relevant standardised residuals are reported in Table 5(a). These standardised residuals were determined using the residual variances estimated in Section 3.1.2.

Assuming $\alpha = 5\%$, the confidence interval is $[z_{\alpha/2} = -1.96, z_{1-\alpha/2} = 1.96]$. All the residuals are outside this interval, but the ‘prime suspect’ is s_{13} , being the sensor with the highest residual (absolute) value. s_{13} is then excluded and, repeating the localisation, the new output is $P \equiv (-81.2, 1345.3, 358.2)$ [mm]. Despite this exclusion, all the residuals continue to be outside the confidence interval. In this other case the sensor with the

highest residual (absolute) value is s_{12} , which is in turn excluded and the localisation is repeated [see Table 5(b)]. The new output is $P \equiv (353.5, 694.9, 562.6)$ [mm] and all the standardised residuals are eventually contained within the confidence interval [see Table 5(c)].

Table 5 Standardised residuals for the measurement exemplified in Section 3.1.2, (a) initial data (b) data after the exclusion of sensor s_{12} (c) data after the exclusion of sensors s_{12} and s_{13}

<i>Sensor</i>	$z_{d_{ij}}$	$z_{\theta_{ij}}$	$z_{\varphi_{ij}}$
<i>(a) Initial data</i>			
s_{11}	136.49	N/A	N/A
s_{12}	(Wrong) -149.21	N/A	N/A
s_{13}	(Wrong) -206.22	N/A	N/A
s_{14}	-47.54	N/A	N/A
s_{15}	145.95	N/A	N/A
s_{21}	N/A	65.46	-41.44
s_{22}	N/A	-80.61	-32.47
s_{23}	N/A	-13.96	4.22
<i>(b) s_{13} excluded</i>			
s_{11}	48.04	N/A	N/A
s_{12}	(Wrong) -241.97	N/A	N/A
s_{14}	-121.6	N/A	N/A
s_{15}	66.74	N/A	N/A
s_{21}	N/A	56.36	-24.54
s_{22}	N/A	-71.01	-13.74
s_{23}	N/A	-10.18	17.63
<i>(c) s_{12} and s_{13} excluded</i>			
s_{11}	0.76	N/A	N/A
s_{14}	0.79	N/A	N/A
s_{15}	0.25	N/A	N/A
s_{21}	N/A	-0.03	-0.05
s_{22}	N/A	1.33	-0.73
s_{23}	N/A	1.21	0.92

Not surprisingly, the global test – which can be performed using the local measurements from the six remaining sensors only – is satisfied; precisely, $SRSS(P) = 5.9 \leq \chi^2_{v=9, 1-\alpha=0.95} \equiv 16.9$.

3.2.3 Second application example

Returning to the example presented in Section 3.1.3 – in which the two angles measured by the laser-tracker angular sensor (s_{22}) are distorted – the relevant standardised residuals are reported in Table 5(a). For this standardisation, we used the residual variances ($\sigma_{d_1}^2$, $\sigma_{\theta_2}^2$ and $\sigma_{\varphi_2}^2$) that are reported in Section 3.1.3.

Table 6 Standardised residuals for the measurement exemplified in Section 3.2.2, (a) initial data (b) data after the exclusion of sensor s_{22}

Sensor	$z_{d_{ij}}$	$z_{\theta_{ij}}$	$z_{\varphi_{ij}}$
<i>(a) Initial data</i>			
s_{11}	N/A	2.15	-9.67
s_{12}	N/A	39.15	-32.44
s_{13}	N/A	-19.87	-22.01
s_{21}	-0.01	N/A	N/A
s_{22}	N/A	(Wrong) 74.64	(Wrong) 36.11
<i>(b) s_{22} excluded</i>			
s_{11}	N/A	0.69	-1.23
s_{12}	N/A	-0.57	-0.11
s_{13}	N/A	-0.31	1.66
s_{21}	$-1.2 * 10^{-4}$	N/A	N/A

Assuming $\alpha = 5\%$, the confidence interval is $[z_{\alpha/2} = -1.96, z_{1-\alpha/2} = 1.96]$. All the residuals are outside this interval, but the ‘prime suspect’ is s_{22} , being the sensor with the highest residual (absolute) value. s_{22} is then excluded and, repeating the localisation, the new output is $P \equiv (1,952.3, 1,250.3, 966.8)$ [mm] and all the standardised residuals are now contained within the confidence interval [see Table 5(b)].

Not surprisingly, the global test – which can be performed using the local measurements from the four remaining sensors – is also satisfied: $SRSS(P) = 4.91 \leq \chi^2_{v=7, 1-\alpha=0.95} \cong 14.1$.

4 Conclusions

The online diagnostics presented in the paper makes it possible to monitor the target-localisation consistency in real time, on the basis of some statistical tests. Tests are deliberately general and can be applied to any combination of LVM systems in which sensors (of different nature) perform distance and/or angular measurements. An important characteristic of these tests is their ability to selectively exclude faulty sensor(s), without interrupting the measurement process.

The proposed tests require the estimation of some parameters; primarily the variances related to the local-measurement residuals. These parameters can be evaluated empirically by performing some preliminary measurements under controlled conditions, according to the reasonable assumption of absence of time or spatial/directional effects. Data collected during the system set-up and calibration can be used for this purpose, with no additional effort (Bar-Shalom et al., 2001).

Since the online implementation of these tests requires a certain computational capacity, it could slow down the target-localisation process. However, this consequence is minimised due to

- 1 the high capacity of existing processors
- 2 the fact that the localisation model in use is linearised
- 3 test segmentation (i.e., the local test is performed only after the global test has detected the presence of potential anomalies).

Some experimental tests showed that the response time required to implement these tests for individual measurements is in the order of magnitude of a few tenths of a second.

The proposed diagnostic tests can be applied in the localisation of a unique target, which is seen by the sensors in use. In the absence of a *universal* target – i.e., a target able to be seen by sensors of different nature simultaneously (such as a laser tracker and a set of photogrammetric cameras) – it is possible to perform the localisation using different targets (such as a SMR for a laser tracker and a reflective spherical target for a set of photogrammetric cameras), repositioning them separately on the same support base. In this way, the local-measurement collection process is split into different phases, which involve sensors of different nature separately (e.g., the local measurements by photogrammetric cameras are collected in one phase, while those by laser tracker are collected in another one). This operation is not problematic for static measurements – in which the target(s) support base is fixed – but it is not feasible for dynamic measurements. Regarding the future, we plan to extend these tests and the proposed mathematical model for target-localisation to the so-called 6-DOF probes equipped with multiple targets, which are visible from sensors of different nature (Maisano and Mastrogiacomo, 2018a, 2018b).

Acknowledgements

This research was supported by the project Co-LVM ‘Cooperative multi-sensor data fusion for enhancing large-volume metrology applications’, which is financed by Fondazione CRT, under the initiative ‘La Ricerca dei Talenti’.

References

- Automated Precision Inc. (API) (2016) *RadianTM* [online] <http://www.apisensor.com> (accessed 24 March 2016).
- Bai, O., Franceschini, F., Galetto, M., Mastrogiacomo, L. and Maisano, D. (2014) ‘A comparison of two different approaches to camera calibration in LSDM photogrammetric systems’, in *American Society of Mechanical Engineers (ASME) 2014 12th Biennial Conference on Engineering Systems Design and Analysis*.
- Bar-Shalom, Y., Li, X.R. and Kirubarajan, T. (2001) *Estimation with Applications to Tracking and Navigation*, Wiley, New York.
- Chen, Z. et al. (2015) ‘A framework of measurement assisted assembly for wing-fuselage alignment based on key measurement characteristics’, *International Journal of Manufacturing Research*, Vol. 10, No. 2, pp.107–128.
- Estler, W.T., Edmundson, K.L., Peggs, G.N. and Parker, D.H. (2002) ‘Large-scale metrology – an update’, *CIRP Ann. Manuf. Technol.*, Vol. 51, No. 2, pp.587–609.
- Franceschini, F. and Maisano, D. (2014) ‘The evolution of large-scale dimensional metrology from the perspective of scientific articles and patents’, *The International Journal of Advanced Manufacturing Technology*, Vol. 70, Nos. 5–8, pp.887–909.

- Franceschini, F., Galetto, M., Maisano, D. and Mastrogiacomo, L. (2009) 'On-line diagnostics in the mobile spatial coordinate measuring system (MScMS)', *Precision Engineering*, Vol. 33, No. 4, pp.408–417.
- Franceschini, F., Galetto, M., Maisano, D. and Mastrogiacomo, L. (2016) 'Combining multiple large volume metrology systems: competitive versus cooperative data fusion', *Precision Engineering*, Vol. 43, pp.514–524.
- Franceschini, F., Galetto, M., Maisano, D., Mastrogiacomo, L. and Pralio, B. (2011) *Distributed Large-Scale Dimensional Metrology*, Springer, London.
- Franceschini, F., Maisano, D. and Mastrogiacomo, L. (2014) 'Cooperative diagnostics for distributed large-scale dimensional metrology systems based on triangulation', *Proceedings of the Institution of Mechanical Engineers, Part B: Journal of Engineering Manufacture*, Vol. 228, No. 4, pp.479–492.
- Franceschini, F., Maisano, D., Mastrogiacomo, L. and Pralio, B. (2010) 'Ultrasound transducers for large-scale metrology: a performance analysis for their use by the MScMS', *Instrumentation and Measurement, IEEE Transactions*, Vol. 59, No. 1, pp.110–121.
- Galetto, M., Mastrogiacomo, L., Maisano, D. and Franceschini, F. (2015) 'Cooperative fusion of distributed multi-sensor LVM (Large Volume Metrology) systems', *CIRP Annals – Manufacturing Technology*, Vol. 64, No. 1, pp.483–486.
- Gertler, J.J. (1998) *Fault Detection and Diagnosis in Engineering System*, Marcel Dekker, NewYork.
- Hall, B.D. (2004) 'On the propagation of uncertainty in complex-valued quantities', *Metrologia*, Vol. 41, No. 3, p.173.
- Hartley, R. and Zisserman, A. (2003) *Multiple View Geometry in Computer Vision*, 2nd ed., Cambridge University, Cambridge, UK.
- Hitachi Kokusai Electric Inc. (2016) *GigE (Gigabit Ethernet) 3CCD Cameras* [online] <http://www.hitachi-kokusai.co.jp> (accessed 24 March 2016).
- JCGM 200:2008 (2008) *VIM – International Vocabulary of Metrology – Basic and General Concepts and Associated Terms (VIM)*, International Organization for Standardization, Geneva, Switzerland.
- Kariya, T. and Kurata, H. (2004) *Generalized Least Squares*, John Wiley & Sons, New York.
- Maisano, D. and Mastrogiacomo, L. (2016) 'A new methodology to design multi-sensor networks for distributed large-volume metrology systems based on triangulation', *Precision Engineering*, Vol. 43, pp.105–118.
- Maisano, D. and Mastrogiacomo, L. (2018a) 'A novel multi-target modular probe for multiple large-volume metrology systems', *To appear on Precision Engineering*, DOI: 10.1016/j.precisioneng.2017.08.017.
- Maisano, D. and Mastrogiacomo, L. (2018b) 'Multi-target modular probe for large-volume metrology', *To appear on Recent Patents on Engineering*, DOI: 10.2174/1872212111666170726155114.
- Maisano, D.A., Jamshidi, J., Franceschini, F., Maropoulos, P.G., Mastrogiacomo, L., Mileham, A., and Owen, G. (2008) 'Indoor GPS: system functionality and initial performance evaluation', *International Journal of Manufacturing Research*, Vol. 3, No. 3, pp.335–349.
- Maropoulos, P.G., Muelaner, J.E., Summers, M.D. and Martin, O.C. (2014) 'A new paradigm in large-scale assembly – research priorities in measurement assisted assembly', *The International Journal of Advanced Manufacturing Technology*, Vol. 70, Nos. 1–4, pp.621–633.
- Peggs, G.N., Maropoulos, P.G., Hughes, E.B., Forbes, A.B., Robson, S., Ziebart, M. and Muralikrishnan, B. (2009) 'Recent developments in large-scale dimensional metrology', *Proceedings of the Institution of Mechanical Engineers, Part B: Journal of Engineering Manufacture*, Vol. 223, No. 6, pp.571–595.

- Ross, S.M. (2009) *Introduction to Probability and Statistics for Engineers and Scientists*, Academic Press, Amsterdam.
- Schmitt, R.H., Peterek, M., Morse, E., Knapp, W., Galetto, M., Härtig, F. and Estler, W.T. (2016) ‘Advances in large-scale metrology – review and future trends’, *CIRP Annals-Manufacturing Technology*, Vol. 65, No. 2, pp.643–665.
- Wieser, A., Petovello, M. and Lachapelle, G. (2004) ‘Failure scenarios to be considered with kinematic high precision relative GNSS positioning’, *Proc. ION GNSS 2004*, 21–24 September, Long Beach, California, pp.1448–1459.
- Wolberg, J. (2005) *Data Analysis Using the Method of Least Squares: Extracting the Most Information from Experiments*, Springer, ISBN 3-540-25674-1.

Appendix

A1 Details on the mathematical model for target localisation

This section presents a detailed description of the mathematical model for target localisation, when adopting combinations of LVM systems.

Let us consider a set of LVM systems (S_i , being $i = 1, 2, \dots$), each of which is equipped with a number of sensors (s_{ij} , being $j = 1, 2, \dots$) that are positioned around the object to be measured, with a local Cartesian coordinate system ($o_{ij}x_{ij}y_{ij}z_{ij}$), which is roto-translated with respect to a global Cartesian coordinate system $OXYZ$ (see Figure A1). The single LVM systems can be *centralised* or *distributed*; in the former case, sensors are rigidly connected to each other, while in the latter, they are not.

A general transformation between a local and the global coordinate system is:

$$\mathbf{X} = \mathbf{R}_{ij} \mathbf{x}_{ij} + \mathbf{X}_{0ij} \Rightarrow \begin{bmatrix} X \\ Y \\ Z \end{bmatrix} = \begin{bmatrix} r_{11ij} & r_{12ij} & r_{13ij} \\ r_{21ij} & r_{22ij} & r_{23ij} \\ r_{31ij} & r_{32ij} & r_{33ij} \end{bmatrix} \begin{bmatrix} x_{ij} \\ y_{ij} \\ z_{ij} \end{bmatrix} + \begin{bmatrix} X_{0ij} \\ Y_{0ij} \\ Z_{0ij} \end{bmatrix} \quad (\text{A1})$$

\mathbf{R}_{ij} is a rotation matrix, which elements are functions of three rotation parameters:

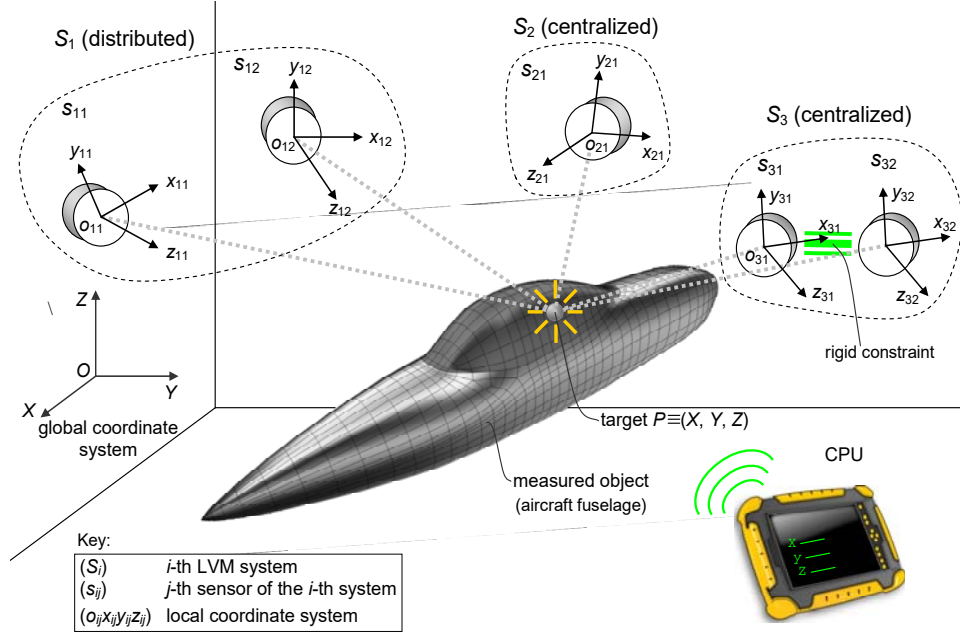
$$\mathbf{R}_{ij} = \begin{bmatrix} \cos\phi_{ij} \cos\kappa_{ij} & -\cos\phi_{ij} \sin\kappa_{ij} & \sin\phi_{ij} \\ \cos\omega_{ij} \sin\kappa_{ij} + \sin\omega_{ij} \sin\phi_{ij} \cos\kappa_{ij} & \cos\omega_{ij} \cos\kappa_{ij} - \sin\omega_{ij} \sin\phi_{ij} \sin\kappa_{ij} & -\sin\omega_{ij} \cos\phi_{ij} \\ \sin\omega_{ij} \sin\kappa_{ij} - \cos\omega_{ij} \sin\phi_{ij} \cos\kappa_{ij} & \sin\omega_{ij} \cos\kappa_{ij} + \cos\omega_{ij} \sin\phi_{ij} \sin\kappa_{ij} & \cos\omega_{ij} \cos\phi_{ij} \end{bmatrix} \quad (\text{A2})$$

where ω_{ij} represents a counterclockwise rotation around the x_{ij} axis; ϕ_{ij} represents a counterclockwise rotation around the new y_{ij} axis, which was rotated by ω_{ij} ; κ_{ij} represents a counterclockwise rotation around the new z_{ij} axis, which was rotated by ω_{ij} and then ϕ_{ij} ; for details, see (Franceschini et al., 2014).

$\mathbf{X}_{0ij} = [X_{0ij}, Y_{0ij}, Z_{0ij}]^T$ are the coordinates of the origin of $o_{ij}x_{ij}y_{ij}z_{ij}$, in the global coordinate system $OXYZ$.

The (six) location/orientation parameters related to each (ij)th sensor (i.e., $X_{0ij}, Y_{0ij}, Z_{0ij}, \omega_{ij}, \phi_{ij}, \kappa_{ij}$) are treated as known parameters, since they are measured in an initial calibration process. This process, which may vary depending on the specific technology of the individual measuring systems, generally includes multiple measurements of calibrated artefacts, within the measurement volume (Bai et al., 2014).

Figure A1 Schematic representation of the combination of three LVM systems: S_1 is a distributed system with two sensors (s_{11} and s_{12}), while S_2 and S_3 are two centralised systems with one sensor (s_{21}) and two sensors (s_{31} and s_{32}) respectively (see online version for colours)



The above considerations apply to both *distributed* and *centralised* LVM systems. In the latter case, sensors are rigidly connected (e.g., consider a photogrammetric tracking bar with three cameras), i.e., the position vectors of the individual sensors (X_{0ij}) are linked to the respective R_{ij} matrices (rigid-body constraint).

The problem of localising the point $P = [X, Y, Z]^T$ can be decomposed by considering distance and angular sensors separately, as discussed in Sections A1.1 and A1.2 respectively.

A1.1 Distance sensors

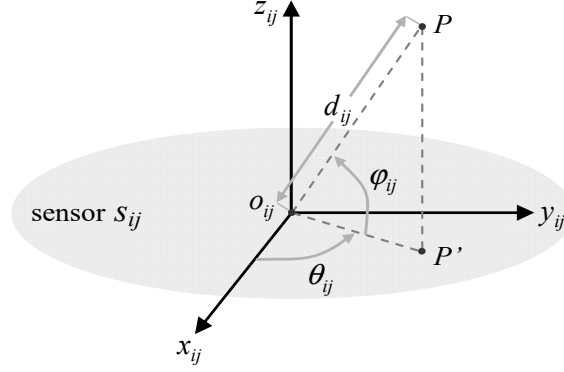
From the local perspective of a generic $(ij)^{\text{th}}$ distance sensor, the distance between $P = [X, Y, Z]^T$ and a local observation point – which is assumed to be coincident with the origin $o_{ij} = [X_{0ij}, Y_{0ij}, Z_{0ij}]^T$ of the local coordinate system $o_{ij}x_{ij}y_{ij}z_{ij}$ – can be calculated as (see Figure A2):

$$d_{ij} = \|X - X_{0ij}\| = \sqrt{(X - X_{0ij})^2 + (Y - Y_{0ij})^2 + (Z - Z_{0ij})^2} \quad (\text{A3})$$

Squaring both terms, we obtain

$$(X - X_{0ij})^2 + (Y - Y_{0ij})^2 + (Z - Z_{0ij})^2 - d_{ij}^2 = \quad (\text{A4})$$

Figure A2 For a generic sensor (s_{ij}), a distance (d_{ij}) and two angles – i.e., θ_{ij} (azimuth) and φ_{ij} (elevation) – are subtended by a line joining the point P (to be localised) and the origin o_{ij} of the local coordinate system $o_{ij}x_{ij}y_{ij}z_{ij}$



Considering a point $\hat{X} = [\hat{X}, \hat{Y}, \hat{Z}]^T$ that is reasonably close to X , equation (A4) can be linearised by a first order Taylor expansion²:

$$2 \cdot \begin{bmatrix} \hat{X} - X_{0ij} \\ \hat{Y} - Y_{0ij} \\ \hat{Z} - Z_{0ij} \end{bmatrix}^T \cdot \begin{bmatrix} X - \hat{X} \\ Y - \hat{Y} \\ Z - \hat{Z} \end{bmatrix} = d_{ij}^2 - \left\{ \left(\hat{X} - X_{0ij} \right)^2 + \left(\hat{Y} - Y_{0ij} \right)^2 + \left(\hat{Z} - Z_{0ij} \right)^2 \right\} = 0 \quad (\text{A5})$$

The above equation can be expressed in matrix form as:

$$\mathbf{A}_{ij}^{dist} \cdot \mathbf{X} - \mathbf{B}_{ij}^{dist} = 0 \quad (\text{A6})$$

where $\mathbf{A}_{ij}^{dist} = 2 \cdot \begin{bmatrix} \hat{X} - X_{0ij} \\ \hat{Y} - Y_{0ij} \\ \hat{Z} - Z_{0ij} \end{bmatrix}^T$ and $\mathbf{B}_{ij}^{dist} = d_{ij}^2 + \hat{X}^2 - X_{0ij}^2 + \hat{Y}^2 - Y_{0ij}^2 + \hat{Z}^2 - Z_{0ij}^2$.

A1.2 Angular sensors

From the local perspective of a generic (ij)th angular sensor, two angles – i.e., θ_{ij} (azimuth) and φ_{ij} (elevation) – are subtended by the line passing through P and o_{ij} (see Figure A2). Precisely, θ_{ij} describes the inclination of segment $o_{ij}P$ with respect to the plane $x_{ij}y_{ij}$ (with a positive sign when $z_{ij} > 0$), while φ_{ij} describes the counterclockwise rotation of the projection ($o_{ij}P'$) of $o_{ij}P$ on the $x_{ij}y_{ij}$ plane, with respect to the x_{ij} axis. Referring to the local coordinate system of the (ij)th sensor, the following relationships hold:

$$\theta_{ij} = \tan^{-1} \frac{y_{ij}}{x_{ij}} \begin{cases} \text{if } x_{ij} \geq 0 \text{ then } -\frac{\pi}{2} \leq \theta_{ij} \leq \frac{\pi}{2} \\ \text{if } x_{ij} < 0 \text{ then } \frac{\pi}{2} < \theta_{ij} < \frac{3\pi}{2} \end{cases} \quad (\text{A7})$$

$$\varphi_{ij} = \sin^{-1} \frac{z_{ij}}{o_{ij}P} \begin{cases} -\frac{\pi}{2} \leq \varphi_{ij} \leq \frac{\pi}{2} \end{cases}$$

Given that:

$$\tan \theta_{ij} = \frac{\sin \theta_{ij}}{\cos \theta_{ij}} \quad (\text{A8})$$

and

$$o_{ij}P = \frac{o_{ij}P'}{\cos \varphi_{ij}} = \frac{x_{ij}/\cos \theta_{ij}}{\cos \varphi_{ij}} = \frac{x_{ij}}{\cos \theta_{ij} \cdot \cos \varphi_{ij}} \quad (\text{A9})$$

Equation (A7) can be reformulated as:

$$\begin{aligned} x_{ij} \cdot \sin \theta_{ij} - y_{ij} \cdot \cos \theta_{ij} &= 0 \\ x_{ij} \cdot \sin \varphi_{ij} - z_{ij} \cdot \cos \theta_{ij} \cdot \cos \varphi_{ij} &= 0 \end{aligned} \quad (\text{A10})$$

In matrix form, equation (A10) becomes:

$$\mathbf{M}_{ij} \mathbf{x}_{ij} = \begin{bmatrix} \sin \theta_{ij} & -\cos \theta_{ij} & 0 \\ \sin \varphi_{ij} & 0 & -\cos \theta_{ij} \cdot \cos \varphi_{ij} \end{bmatrix} \cdot \begin{bmatrix} x_{ij} \\ y_{ij} \\ z_{ij} \end{bmatrix} = 0 \quad (\text{A11})$$

The system of two equations in equation (A11) can be expressed as a function of the global coordinates of point P . Reversing equation (A1), for switching from the local to the global coordinates, and considering that \mathbf{R}_{ij} is orthonormal – therefore $\mathbf{R}_{ij}^{-1} = \mathbf{R}_{ij}^T$ (Hartley and Zisserman, 2003) – we obtain:

$$\mathbf{x}_{ij} = \mathbf{R}_{ij}^{-1} (\mathbf{X} - \mathbf{X}_{0_{ij}}) = \mathbf{R}_{ij}^T (\mathbf{X} - \mathbf{X}_{0_{ij}}) \quad (\text{A12})$$

Combining equations (A11) and (A12), we obtain:

$$\mathbf{M}_{ij} \mathbf{R}_{ij}^T (\mathbf{X} - \mathbf{X}_{0_{ij}}) = 0 \quad (\text{A13})$$

from which:

$$\mathbf{M}_{ij} \mathbf{R}_{ij}^T \mathbf{X} - \mathbf{M}_{ij} \mathbf{R}_{ij}^T \mathbf{X}_{0_{ij}} = 0 \quad (\text{A14})$$

We note that the equations of this system are linear with respect to the three (unknown) coordinates of P . Equation (A14) can be expressed in compact form, as:

$$\mathbf{A}_{ij}^{ang} \cdot \mathbf{X} - \mathbf{B}_{ij}^{ang} = 0 \quad (\text{A15})$$

being $\mathbf{A}_{ij}^{ang} = \mathbf{M}_{ij} \mathbf{R}_{ij}^T$ and $\mathbf{B}_{ij}^{ang} = \mathbf{M}_{ij} \mathbf{R}_{ij}^T \mathbf{X}_{0_{ij}}$.

The matrix expression in equation (A15) is similar to the one related to distance sensors [in equation (A6)]. However, in the case of distance sensors, it encapsulates a single equation, while in the case of angular sensors, it encapsulates two equations.

A1.3 Note on hybrid sensors

A particular case is represented by *hybrid* sensors, which can be seen as special sensors integrating a distance sensor and an angular sensor (e.g., the sensors of a laser tracker/tracer). For these sensors, the usable equations for the localisation problem are three: one related to a distance measurement (\hat{d}_{ij}) and two related to angular measurements ($\hat{\theta}_{ij}, \hat{\varphi}_{ij}$). These equations can be aggregated into a single linear system:

$$\mathbf{A}_{ij}^{hyb} \cdot \mathbf{X} - \mathbf{B}_{ij}^{hyb} = \begin{bmatrix} \mathbf{A}_{ij}^{dist} \\ \mathbf{A}_{ij}^{ang} \end{bmatrix} \cdot \mathbf{X} - \begin{bmatrix} \mathbf{B}_{ij}^{dist} \\ \mathbf{B}_{ij}^{ang} \end{bmatrix} = 0 \quad (\text{A16})$$

where the superscript ‘*hyb*’ stands for hybrid and $\mathbf{A}_{ij}^{dist}, \mathbf{B}_{ij}^{dist}, \mathbf{A}_{ij}^{ang}$ and \mathbf{B}_{ij}^{ang} are the same matrices illustrated in Sections A1.1 and A1.2.

The same system can be formulated in an alternative way. The (unknown) coordinates of P , with respect to the (same) local reference system related to the distance and the angular sensors are given by (see Figure A2):

$$\begin{cases} x_{ij} = d_{ij} \cdot \cos \varphi_{ij} \cdot \cos \theta_{ij} \\ y_{ij} = d_{ij} \cdot \cos \varphi_{ij} \cdot \sin \theta_{ij} \\ z_{ij} = d_{ij} \cdot \sin \varphi_{ij} \end{cases} \quad (\text{A17})$$

Combining equations (A1) and (A17) we obtain:

$$\mathbf{R}_{ij}^T \mathbf{X} - \mathbf{R}_{ij}^T \mathbf{X}_{0_{ij}} = [d_{ij} \cdot \cos \varphi_{ij} \cdot \cos \theta_{ij} \quad d_{ij} \cdot \cos \varphi_{ij} \cdot \sin \theta_{ij} \quad d_{ij} \cdot \sin \varphi_{ij}]^T \quad (\text{A18})$$

We note that the equations of this system are linear with respect to the three (unknown) coordinates of P and can be expressed in compact form as:

$$\mathbf{A}_{ij}^{hyb} \cdot \mathbf{X} - \mathbf{B}_{ij}^{hyb} = 0 \quad (\text{A19})$$

where $\mathbf{A}_{ij}^{hyb} = \mathbf{R}_{ij}^T$ and $\mathbf{B}_{ij}^{hyb} = [d_{ij} \cdot \cos \varphi_{ij} \cdot \cos \theta_{ij} \quad d_{ij} \cdot \cos \varphi_{ij} \cdot \sin \theta_{ij} \quad d_{ij} \cdot \sin \varphi_{ij}]^T + \mathbf{R}_{ij}^T \mathbf{X}_{0_{ij}}$.

The expression in equation (A19) is certainly simpler and more compact than that in equation (A16); however, it has a significant limitation: the three equations that it encapsulates [shown in equation (A17)] are coupled to each other, as they require the simultaneous knowledge of d_{ij} , θ_{ij} and φ_{ij} . For example, in the case d_{ij} only is available, while θ_{ij} and φ_{ij} not, none of the three equations can be used. For this reason, it seems more practical to use the formulation in equation (A16)³, in which the distance and angular measurements are treated separately.

A1.4 Weighting and solution

Considering a generic combination of LVM systems that are equipped with distance and/or angular sensors, the resulting linearised target-localisation model is:

$$\mathbf{A} \cdot \mathbf{X} - \mathbf{B} = \begin{bmatrix} \mathbf{A}^{dist} \\ \mathbf{A}^{ang} \end{bmatrix} \cdot \mathbf{X} - \begin{bmatrix} \mathbf{B}^{dist} \\ \mathbf{B}^{ang} \end{bmatrix} = 0 \quad (\text{A20})$$

where blocks \mathbf{A}^{dist} , \mathbf{A}^{ang} , \mathbf{B}^{dist} and \mathbf{B}^{ang} are defined as:

$$\mathbf{A}^{dist} = \begin{bmatrix} \vdots \\ \mathbf{A}_{ij}^{dist} \\ \vdots \end{bmatrix}_{ij \in I^{dist}}, \quad \mathbf{A}^{ang} = \begin{bmatrix} \vdots \\ \mathbf{A}_{ij}^{ang} \\ \vdots \end{bmatrix}_{ij \in I^{ang}}, \quad \mathbf{B}^{dist} = \begin{bmatrix} \vdots \\ \mathbf{B}_{ij}^{dist} \\ \vdots \end{bmatrix}_{ij \in I^{dist}}, \quad \mathbf{B}^{ang} = \begin{bmatrix} \vdots \\ \mathbf{B}_{ij}^{ang} \\ \vdots \end{bmatrix}_{ij \in I^{ang}}$$

where I^{dist} and I^{ang} are the sets of index-pair values (ij) relating to the distance and angular sensors respectively.

The system in equation (20) can be solved when at least three equations are available (e.g., P is seen by at least three distance sensors, or one distance sensor and one angular sensor, or two angular sensors, etc.). Since this system is generally overdefined (more equations than unknown parameters), there are several possible solution approaches, ranging from those based on the iterative minimisation of a suitable error function (Franceschini et al., 2014) to those based on the least squares method (Wolberg, 2005).

It is worth remarking that the equations of the system may differently contribute to the uncertainty in the localisation of P . Specifically, two of the main factors affecting this uncertainty are:

- *Uncertainty in the local measurements* (\hat{d}_{ij} , $\hat{\theta}_{ij}$ and $\hat{\phi}_{ij}$), which generally depends on the metrological characteristics of sensors.
- *Relative position* between the point to be localised (P) and each (ij)th sensor; e.g., assuming that the uncertainty in angular measurements is fixed, the uncertainty in the localisation of P tends to increase proportionally to the *distance* between P and the angular sensors (Maisano and Mastrogiacomo, 2016).
- *Uncertainty in the position/orientation of sensors* (\hat{X}_{0ij} , \hat{Y}_{0ij} , \hat{Z}_{0ij} , $\hat{\omega}_{ij}$, \hat{j}_{ij} and \hat{k}_{ij}), resulting from initial calibration process(es).

For simplicity, the proposed mathematical model considers only the first two factors, neglecting the third one (Maisano and Mastrogiacomo, 2016).

The sensors that mostly contribute to uncertainty in the localisation of P are therefore the less accurate and/or the more distant from P .

Returning to the system in equation (A20), it would be appropriate to solve it giving greater weight to the contributions from sensors that produce less uncertainty and *vice versa*. To this purpose, an elegant and practical method is that of the GLS (Kariya and Kurata, 2004), in which a weight matrix (\mathbf{W}), which takes into account the uncertainty produced by the equations of the system. One of the most practical ways to define \mathbf{W} is the application of the multivariate law of propagation of uncertainty to the system in equation (A20), referring to the parameters affected by uncertainty (Hall,

2004). Assuming that such parameters are the distances or angles measured by each $(ij)^{\text{th}}$ sensor, we collect them in a vector ξ :

$$\xi = \begin{bmatrix} \xi^{dist} \\ \xi^{ang} \end{bmatrix} = \begin{bmatrix} \begin{bmatrix} \vdots \\ d_{ij} \\ \vdots \end{bmatrix}_{ij \in I^{dist}} \\ \begin{bmatrix} \vdots \\ \begin{pmatrix} \theta_{ij} \\ \phi_{ij} \end{pmatrix} \\ \vdots \end{bmatrix}_{ij \in I^{ang}} \end{bmatrix} \quad (\text{A22})$$

We remark that ξ is a vector containing the sensor local measurements, which can be decomposed in the two sub-vectors, ξ^{dist} and ξ^{ang} , the former relating to distance sensors and the latter to angular sensors. For simplicity, we do not take into account the uncertainty related to the estimates of the location/orientation parameters of the sensors, which are contained in $X_{0_{ij}}$ and R_{ij} (Franceschini et al., 2011).

Propagating the uncertainty of the equations in equation (A20) with respect to the elements in ξ , we define W as:

$$W = \left[J \cdot (\text{cov}(\xi)) \cdot J^T \right]^{-1}. \quad (\text{A23})$$

Let us now focus the attention on the elements in the second member of equation (A23). J is the Jacobian (block-diagonal) matrix containing the partial derivatives of the elements in the first member of equation (A20) with respect to the elements in ξ :

$$J = \begin{bmatrix} J^{dist} & \mathbf{0} \\ \mathbf{0} & J^{ang} \end{bmatrix} = \begin{bmatrix} \begin{bmatrix} \ddots & & \mathbf{0} \\ & J_{ij}^{dist} & \\ \mathbf{0} & & \ddots \end{bmatrix}_{ij \in I^{dist}} & \mathbf{0} \\ \mathbf{0} & \begin{bmatrix} \ddots & & \mathbf{0} \\ & J_{ij}^{ang} & \\ \mathbf{0} & & \ddots \end{bmatrix}_{ij \in I^{ang}} \end{bmatrix} \quad (\text{A24})$$

where blocks J_{ij}^{dist} and J_{ij}^{ang} are defined as

$$\begin{aligned} J_{ij}^{dist} &= [2 \cdot d_{ij}] \\ J_{ij}^{ang} &= \begin{bmatrix} x_{ij} \cdot \cos \theta_{ij} + y_{ij} \cdot \sin \theta_{ij} & 0 \\ z_{ij} \cdot \sin \theta_{ij} \cdot \cos \phi_{ij} & x_{ij} \cos \phi_{ij} + z_{ij} \cdot \cos \theta_{ij} \cdot \sin \phi_{ij} \end{bmatrix} \end{aligned} \quad (\text{A25})$$

and the remaining elements of the matrix are all zeros.

Returning to the description of equation (A22), $\text{cov}(\xi)$ is the covariance matrix of ξ , defined as:

$$\mathbf{cov}(\xi) = \begin{bmatrix} \mathbf{cov}(\xi^{dist}) & \mathbf{0} \\ \mathbf{0} & \mathbf{cov}(\xi^{ang}) \end{bmatrix} = \begin{bmatrix} \begin{bmatrix} \ddots & & \mathbf{0} \\ & \mathbf{cov}(\xi_{ij}^{dist}) & \\ \mathbf{0} & \ddots & \end{bmatrix}_{ij \in J^{dist}} & \mathbf{0} \\ \mathbf{0} & \begin{bmatrix} \ddots & & \mathbf{0} \\ & \mathbf{cov}(\xi_{ij}^{ang}) & \\ \mathbf{0} & \ddots & \end{bmatrix}_{ij \in J^{ang}} \end{bmatrix} \quad (\text{A26})$$

where blocks $\mathbf{cov}(\xi_{ij}^{dist})$ and $\mathbf{cov}(\xi_{ij}^{ang})$ are defined as

$$\begin{aligned} \mathbf{cov}(\xi_{ij}^{dist}) &= \begin{bmatrix} \sigma_{d_{ij}}^2 \end{bmatrix} \\ \mathbf{cov}(\xi_{ij}^{ang}) &= \begin{bmatrix} \sigma_{\theta_{ij}}^2 & 0 \\ 0 & \sigma_{\phi_{ij}}^2 \end{bmatrix} \end{aligned} \quad (\text{A27})$$

We notice that the diagonal elements of $\mathbf{cov}(\xi)$ are the variances related to the distances and angles measured by the individual sensors (Section 3.1.1 illustrates some practical ways to estimate these parameters). The off-diagonal entries of these blocks are zeros, assuming no correlation between the local measurements by a generic sensor; the off-block-diagonal entries are zeros, assuming that sensors work independently from each other and there is no correlation between the local measurements related to different sensors.

By applying the GLS method to the system in equation (A20), we obtain the final position estimate of P as:

$$\hat{X} = (A^T \cdot W \cdot A)^{-1} \cdot A^T \cdot W \cdot B \quad (\text{A28})$$

For further details on the GLS method, see (Kariya and Kurata, 2004).

We emphasise that an (at least rough) initial estimate of X is required to define some elements of the blocks A_{ij}^{dist} [see equation (A6)] and J_{ij}^{ang} [see equation (A25)]. This problem can be overcome applying the formula in equation (A28) recursively:

- 1 setting no-matter-what initial \hat{X} , in order to determine the elements of blocks A_{ij}^{dist} and J_{ij}^{ang}
- 2 obtaining a not very accurate localisation of P
- 3 iterating the localisation using the result of the previous one as a new \hat{X} .

We verified that the localisation tends to converge to the correct solution after no more than five-ten iterations.

Notes

- 1 The authors are aware that systematic measurement errors can never be eradicated completely; this assumption is therefore not valid in general, even though could be adequate for the purpose of diagnostics (Franceschini et al., 2014).
- 2 The ‘double-hat’ symbol ‘ $\hat{\hat{\cdot}}$ ’ indicates that a point close to \mathbf{X} can be obtained through a rough estimate of the (final) estimate of \mathbf{X} itself (i.e., $\hat{\hat{\mathbf{X}}}$). We will illustrate how to determine $\hat{\hat{\mathbf{X}}}$ later.
- 3 Extending this reasoning, we also might find the way to decouple the equations relating to the angles (θ_{ij} and φ_{ij}) that are measured by angular sensors [see equation (A7)]. However, this would unnecessarily complicate the formulation of the problem, without any practical reason: in fact, it is very unlikely that the same angular sensor provides a correct measurement for one angle and a wrong one for the other one.